THERMAL-ELECTROCHEMICAL COUPLED MODELING OF A LITHIUM-ION CELL

W.B. Gu and C.Y. Wang
GATE Center for Advanced Energy Storage
Department of Mechanical Engineering & Pennsylvania Transportation Institute
The Pennsylvania State University
University Park, PA 16802, USA

ABSTRACT

A multi-dimensional thermal and electrochemical coupled model is developed for Li-ion batteries. The model is capable of predicting the cell internal temperature distribution as well as the average cell temperature evolution. Numerical simulations are performed for a large-size Li-ion cell for electric vehicle applications. Comparisons between the coupled and decoupled model predictions indicate the importance of thermal-electrochemical coupling for accurate prediction of the thermal and electrochemical behaviors of Li-ion batteries. Numerical results show that large temperature gradients develop along the cell height, causing severe non-uniformity in both electrode reaction rate and electrolyte concentration distributions. Evolutions of cell potential and temperature are found to be greatly affected by the thermal environment and the cell aspect ratio.

INTRODUCTION

Performance and safety are two primary considerations in the design of advanced lithium-ion batteries. The performance of a lithium-ion battery can be greatly influenced by the thermal environment, and its thermal behavior is in turn determined by the electrochemical and chemical processes occurring inside the cell during charge and discharge. Significant temperature gradients may develop when a lithium-ion cell is scaled up for electric vehicle (EV) and hybrid electric vehicle (HEV) applications and, thus current and temperature distributions become two-dimensional.[1] Information on the temperature distribution is essential to capture the hot spot that may trigger thermal runaway thus leading to the failure of a battery.

While experiments are necessary to study the underlying physical chemistry of materials used in lithium-ion batteries and evaluate the battery performance, mathematical models based on first principles are useful in providing a fundamental understanding of the internal transport phenomena and in aiding the optimization of battery design. Fuller et al.[2] first developed an isothermal electrochemical model for a dual-insertion lithium-ion cell and the model predictions were compared to the experimental data with good agreement.[3] Botte et al.[4] recently extended it to a non-isothermal one with an exothermic side reaction taken into account. However, both models are virtually one-dimensional and assumed a uniform cell temperature. Most recently, Baker and Verbrugge[1] performed a two-dimensional asymptotic analysis to a

simplified lithium-ion cell system assuming secondary current distribution and linear kinetics.

A general thermal-electrochemical coupled model[5] has been developed for battery systems based on the previously developed micro-macroscopic modeling approach.[6] The model is multi-dimensional and capable of predicting the temperature distribution inside a cell as well as the overall cell temperature evolution. The model has been applied to simultaneously simulate thermal and electrochemical behaviors of a Ni-MH cell. In the present work, a two-dimensional thermal-electrochemical study is performed by applying this generic model to the lithium-ion system. Solid-state species diffusion is taken into account. As a first step, no side reactions of chemical nature are considered for simplicity. Numerical simulations are performed for a large-size lithium-ion cell intended for EV and HEV applications. Importance of thermal-electrochemical coupling will be illustrated by comparing the coupled and decoupled model predictions. Finally, two-dimensional behaviors of the cell will be numerically explored.
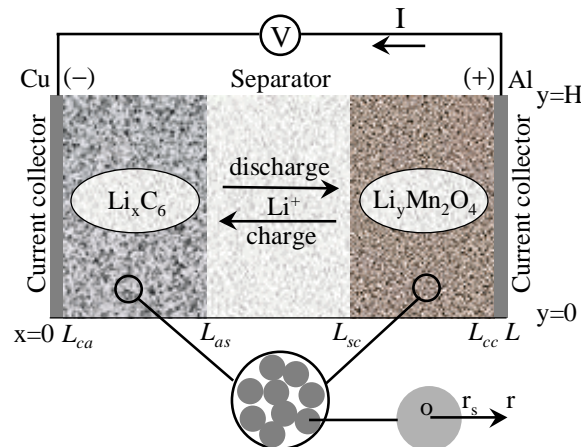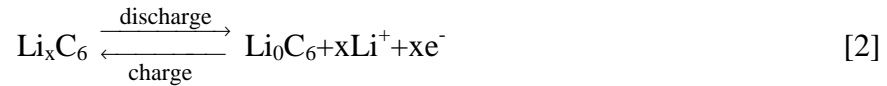
PHYSICAL MODEL

System Description

The lithium-ion cell of interest consists of the negative electrode current collector (Cu), negative electrode (Li_xC_6), separator, positive electrode ($Li_yMn_2O_4$), and the positive electrode current collector (Al), as schematically shown in Fig. 1. The electrolyte is a solution of lithium salt in a non-aqueous solvent. Electrochemical reactions occurring at the electrode/electrolyte interfaces are as follows:

Composite positive electrode

$$Li_{y-x}Mn_2O_4 + xLi^+ + xe^- \underset{\text{charge}}{\overset{\text{discharge}}{\rightleftharpoons}} Li_yMn_2O_4 \qquad [1]$$
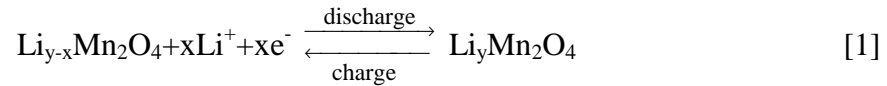
Composite negative electrode

$$Li_xC_6 \underset{\text{charge}}{\overset{\text{discharge}}{\rightleftharpoons}} Li_0C_6 + xLi^+ + xe^- \qquad [2]$$

Fig. 1. Schematic of a lithium-ion cell and model representation.

The current is considered to flow through the tabs on the top of the two electrodes. During discharge, the lithium ions insert into solid particles of the positive electrode and de-insert from solid particles of the negative electrode. Lithium ion diffusion in the solid phase and the electrolyte depletion in the positive electrode are two common limiting mechanisms of cell discharge. Heat is generated within the cell and dissipated to the surroundings in all directions. The worst case in practical situations is, however, that heat is dissipated only through the tabs on the top. As a result, a temperature gradient develops along the cell height, thereby resulting in non-uniform electrode reaction rates.

Assumptions

i. No gas phase is present.
ii. Concentrated binary electrolyte is assumed.[1, 2]
iii. Side reactions, significant only at relatively high temperatures,[4] are ignored.
iv. Charge transfer kinetics follows Butler-Volmer equation.
v. Ionic species transport in the electrolyte is by diffusion and migration only.
vi. The active electrode materials are made up of spherical particles with a uniform size.
vii. Volume change during cell operation is neglected, resulting in constant electrode porosities.
viii. The transport of lithium inside the active material particles is by diffusion with a constant diffusion coefficient.
ix. Interfacial chemical equilibrium exists in the electrolyte phase due to a large value of the mass diffusivity of electrolyte.
x. Interfacial electrical equilibrium exists in both the electrolyte and solid active material phases due to either large values of their electronic conductivities or a small size of active material particles.

MATHEMATICAL FORMULATION

With the above assumptions, a multi-dimensional electrochemical and thermal coupled model for the considered system can be derived based on the previously developed general modeling approach.[5-7] Thus, only the final model equations are summarized below.

Electrode Kinetics

Reaction rates for insertion and de-insertion reactions 1 and 2 are assumed to follow the Butler-Volmer equation,[3] namely

$$\bar{i}_{nj} = i_{oj}\left[\exp\left(\frac{\alpha_{aj}F}{RT}\eta_j\right) - \exp\left(-\frac{\alpha_{cj}F}{RT}\eta_j\right)\right] \qquad [3]$$

where α_{aj} and α_{cj} are the anodic and cathodic transfer coefficients of electrode reaction j, F is the Faraday's constant, R the universal gas constant, and T the absolute temperature in Kelvin. The exchange current density, i_{oj}, is a function of lithium concentrations in both electrolyte and solid active material phases;[3] i.e.

$$i_{oj} = k(c_e)^{\alpha_{aj}} (c_{s,\max} - \bar{c}_{se})^{\alpha_{aj}} (\bar{c}_{se})^{\alpha_{cj}} \qquad [4]$$

where c stands for the volume-averaged lithium concentration, with subscripts e and s referring to the concentration in the electrolyte and solid phases, respectively, $\bar{c}_{se}$ represents the area-averaged solid-state lithium concentration at the electrode/electrolyte interface, and $c_{s,\max}$ is the maximum concentration of lithium in the solid phase. The constant, k, is determined by the initial exchange current density and species concentrations. The local surface overpotential of reaction j, η_j, is defined as[3]

$$\eta_j = \phi_s - \phi_e - U_j - \bar{i}_{nj} R_f \qquad [5]$$

where U_j is the open-circuit potential (OCP) of electrode reaction j and R_f is a finite film resistance on the electrode surface. The passive film, such as the solid-electrolyte interphase (SEI) layer, is formed by irreversible side reactions on the electrode surface. The film resistance was used as an adjustable parameter to get better agreement between simulation and experiment.[3] Its origin has yet to be further explored.[3] Zero value of R_f is used in the present work due to a lack of clear physical justification for R_f.

The OCP is a function of local state of charge (SOC) and temperature. It is usually approximated as a linear function of temperature, namely

$$U_j = U_{j,ref} + (T - T_{ref}) \frac{\partial U_j}{\partial T} \qquad [6]$$

where $U_{j,ref}$ is the OCP at a reference temperature. In the present work, expressions for the open-circuit potentials of manganese dioxide and carbon electrodes at 25 ˚C as given by Doyle et al.[3] are used, i.e.

$$U_{1,ref} = 4.19829 + 0.565661 \tanh[-14.5546\theta + 8.60942]$$
$$- 0.0275479[1/(0.998432 - \theta)^{0.492465} - 1.90111] \qquad [7]$$
$$- 0.157123 \exp(-0.04738\theta^8) + 0.810239 \exp[-40(\theta - 0.133875)]$$

and

$$U_{2,ref} = -0.16 + 1.32 \exp(-3.0\theta) + 10.0 \exp(-2000.0\theta) \qquad [8]$$

where the local SOC, θ, is evaluated using the solid-state lithium concentration at the electrode/electrolyte interface, i.e.

$$\theta = \frac{\bar{c}_{se}}{c_{s,\max}} \qquad [9]$$

The linear temperature dependence of the OCP, $\partial U_j / \partial T$, is not known for the lithium-ion system and has been neglected as a first approximation.[4]

Species Conservation Equations

Conservation of lithium ion in the electrolyte yields

$$\frac{\partial(\varepsilon_e c_e)}{\partial t} = \nabla \cdot \left(D_e^{eff} \nabla c_e\right) + \frac{1 - t_+^o}{F} j^{Li} - \frac{\mathbf{i}_e \cdot \nabla t_+^o}{F} \qquad [10]$$

where t_+^o is the transference number of the Li^+ with respect to the velocity of solvent. Depending on the combination of electrolyte and solvent, it can be a function of the electrolyte concentration. In the present work, a constant value of the transference number of lithium ion is assumed.[3] The last term on the right hand side of Eq. 10 then vanishes. The effective diffusion coefficient including the effect of tortuosity is evaluated by the Bruggeman relation, i.e.

$$D_e^{eff} = D_e \varepsilon_e^{1.5} \qquad [11]$$

where D_e is the mass diffusion coefficient of lithium ion in the electrolyte.

The second term on the RHS of Eq. 10 is proportional to j^{Li}, the transfer current resulting from the lithium insertion or de-insertion reaction at the electrode/electrolyte interface that consumes or generates the species Li^+, namely

$$j^{Li} = \begin{cases} a_{s1} \bar{i}_{n1} & \text{in the } Li_y Mn_2 O_4 \text{ electrode} \\ 0 & \text{in the separator} \\ a_{s2} \bar{i}_{n2} & \text{in the } Li_x C_6 \text{ electrode} \end{cases} \qquad [12]$$

where a_s is the specific interfacial area of an electrode, with subscript 1 and 2 representing the manganese dioxide and carbon electrodes, respectively.

Conservation of lithium in the solid phase yields

$$\frac{\partial(\varepsilon_s c_s)}{\partial t} = \frac{j^{Li}}{F} \qquad [13]$$

The interfacial balance of lithium around either $Li_y Mn_2 O_4$ or $Li_x C_6$ particles is given by

$$\frac{D_s}{l_{se}}(\bar{c}_{se} - c_s) = \frac{j^{Li}}{a_s F} \qquad [14]$$

where l_{se} is the microscopic diffusion length characterizing lithium diffusion in solid active materials. Assuming that an insertion electrode is composed of spherical particles with a radius of r_s, the diffusion length is expressed as[6]

$$l_{se} = \frac{r_s}{5} \qquad [15]$$

For the spherical morphology of an insertion electrode, the specific interfacial area of the electrode is calculated by

$$a_s = \frac{3\varepsilon_s}{r_s} = \frac{3(1 - \varepsilon_e - \varepsilon_p - \varepsilon_f)}{r_s} \qquad [16]$$

where ε_s, ε_e, ε_p, and ε_f are the volume fractions of solid active material, liquid electrolyte, polymer matrix, and conductive filler, respectively.

Charge Conservation Equations

Conservation of charge in the electrolyte results in

$$\nabla \cdot \left(\kappa^{eff} \nabla \phi_e \right) + \nabla \cdot \left(\kappa_D^{eff} \nabla \ln c_e \right) + j^{Li} = 0 \qquad [17]$$

This equation can be used to determine the electrical potential in the electrolyte phase, ϕ_e. Here, the effective ionic conductivity is given by $\kappa^{eff} = \kappa \varepsilon_e^{1.5}$ following the Bruggeman correction for the tortuosity effect, while the diffusional conductivity, κ_D^{eff}, is given by

$$\kappa_D^{eff} = \frac{2RT\kappa^{eff}}{F} \left(t_+^o - 1 \right) \left(1 + \frac{d \ln f_\pm}{d \ln c_e} \right) \qquad [18]$$

where $f_\pm$ is the mean molar activity coefficient of the electrolyte. A constant value of $f_\pm$ is assumed in this work due to a lack of experimental data. The conductivity of the electrolyte is strongly dependent on the electrolyte composition. For the electrolyte consisting of $LiPF_6$ in a 2:1 v/v mixture of ethylene carbonate (EC) and dimethyl carbonate (DMC), it was found that[3]

$$\begin{aligned} \kappa &= 4.1253 \times 10^{-4} + 5.007 c_e - 4.7212 \times 10^3 c_e^2 \\ &\quad + 1.5094 \times 10^6 c_e^3 - 1.6018 \times 10^8 c_e^4 \end{aligned} \qquad [19]$$

Conservation of charge in the solid phase yields

$$\nabla \cdot \left(\sigma^{eff} \nabla \phi_s \right) - j^{Li} = 0 \qquad [20]$$

where the effective conductivity of the solid phase, σ^{eff}, is related to the conductivity of the active materials, σ, by

$$\sigma^{eff} = \varepsilon_s \sigma \qquad [21]$$

where s denotes the manganese dioxide and carbon electrodes, respectively.

Thermal Energy Conservation Equation

Without convection in the cell, the general thermal energy equation[5] reduces to

$$\frac{\partial(\rho c_p T)}{\partial t} = \nabla \cdot \lambda \nabla T + q \qquad [22]$$

where the heat capacity ρc_p and the effective thermal conductivity λ can be calculated from the corresponding component values, i.e.

$$\rho c_p = \sum_k \varepsilon_k \rho_k c_{pk} \qquad [23]$$

and

$$\lambda = \sum_k \varepsilon_k \lambda_k \qquad [24]$$

Note that the effect of tortuosity on the effective thermal conductivity is neglected in Eq. 24. The heat generation rate is expressed by[5]

$$q = a_{sj}\bar{i}_{nj}\left(\phi_s - \phi_e - U_j + T\frac{\partial U_j}{\partial T}\right) + \sigma^{eff}\nabla\phi_s \cdot \nabla\phi_s$$
$$+ (\kappa^{eff}\nabla\phi_e \cdot \nabla\phi_e + \kappa_D^{eff}\nabla\ln c_e \cdot \nabla\phi_e) \qquad [25]$$

While the first term on the RHS of Eq. 25 represents the heat effect due to electrode reactions, the second and third term result from the joule heating in the solid active material and electrolyte phases, respectively. $\partial U_j / \partial T$ (or equivalently the entropy change of the electrode reaction) has been neglected in practice due to a lack of experimental data for Li-ion systems.[1, 4] Such fundamental information is, however, necessary in accurate prediction of the local heat generation rate inside a cell.

Thermal and Electrochemical Coupling

Temperature-dependent physicochemical properties, such as the diffusion coefficient and ionic conductivity of electrolyte, are needed to couple the thermal model with the multiphase mass transport and electrochemical model. More specifically, the dependence of the physiochemical properties on the temperature can be described by the Arrhenius' equation[4, 5]

$$\Phi = \Phi_{ref}\exp\left[\frac{E_{act,\Phi}}{R}\left(\frac{1}{T_{ref}} - \frac{1}{T}\right)\right] \qquad [26]$$

where Φ is a general variable representing the diffusion coefficient of a species, conductivity of the electrolyte, exchange current density of an electrode reaction, etc., with subscript *ref* denoting the value at a reference temperature. $E_{act,\Phi}$ is the activation energy of the evolution process of Φ. Its magnitude determines the sensitivity of Φ to temperature.

The heat generation rate due to electrochemical reactions and joule heating are calculated locally via the foregoing multiphase electrochemical model, and subsequently be used in the thermal energy conservation equation to calculate the temperature field. This temperature information is, in turn, fed back to update the electrochemical

calculations through temperature-dependent physicochemical properties. The thermal and electrochemical behaviors of a battery are thus fully coupled via Eqs. 25 and 26 as well as Eq. 6, the temperature-dependent electrode OCPs.

Table I. Summary of model equations for a Li-Ion battery

Species in liquid phase	$\dfrac{\partial(\varepsilon_e c_e)}{\partial t} = \nabla \cdot \left(D_e^{eff} \nabla c_e\right) + \dfrac{1 - t_+^o}{F} j^{Li} - \dfrac{\mathbf{i}_e \cdot \nabla t_+^o}{F}$	Eq. 10
Species in solid phase	$\dfrac{\partial(\varepsilon_s c_s)}{\partial t} = \dfrac{j^{Li}}{F}$	Eq. 13
	$\dfrac{D_s}{l_{se}}(\overline{c}_{se} - c_s) = \dfrac{j^{Li}}{a_s F}$	Eq. 14
Liquid phase potential	$\nabla \cdot \left(\kappa^{eff} \nabla \phi_e\right) + \nabla \cdot \left(\kappa_D^{eff} \nabla \ln c_e\right) + j^{Li} = 0$	Eq. 17
Solid phase potential	$\nabla \cdot \left(\sigma^{eff} \nabla \phi_s\right) - j^{Li} = 0$	Eq. 20
Temperature	$\dfrac{\partial(\rho c_p T)}{\partial t} = \nabla \cdot \lambda \nabla T + q$	Eq. 22
	$q = a_{sj} \overline{i}_{nj}\left(\phi_s - \phi_e - U_j + T \dfrac{\partial U_j}{\partial T}\right) + \sigma^{eff} \nabla \phi_s \cdot \nabla \phi_s$ $+ (\kappa^{eff} \nabla \phi_e \cdot \nabla \phi_e + \kappa_D^{eff} \nabla \ln c_e \cdot \nabla \phi_e)$	Eq. 25

Summary of Model Equations

In summary, a total of five governing equations, i.e. Eqs. 10, 13, 17, 20, and 22, can be solved for the five unknowns: c_e, c_s, ϕ_e, ϕ_s and T. An additional interfacial balance, Eq. 14, is provided to determine the interfacial concentration of solid-state lithium: $\overline{c}_{se}$. The model equations are summarized in Table I, subject to the following initial and boundary conditions (for two-dimensional simulations).

Initial and Boundary Condition

Initial conditions — Uniform initial conditions are assumed, i.e.

$$c_e = c_e^o, c_s = c_s^o \text{ and } T = T^o \tag{27}$$

Boundary conditions — the computational domain includes the two current collectors, as shown in Fig. 1. The electrolyte is confined within the cell and no reaction occurs at the current collector surfaces, giving rise to

$$\frac{\partial c^{Li}}{\partial n} = 0 \text{ and } \frac{\partial \phi_e}{\partial n} = 0 \tag{28}$$

at all boundaries. Current is applied at the tabs on the top and heat is dissipated only through the tabs (basecase) or through the sides as well as through the tabs, yielding

Table II. Values of parameters used in the simulations[*]

Symbol	Unit	Value					Ref.
		Cu	Anode	Separator	Cathode	Al	
L_i	μm	10	128	76	190	15	1, 3
ρ	g/cm^3	9.0	2.5	1.2	1.5	2.7	1
c_p	J/g·K	0.381	0.7	0.7	0.7	0.870	1
k	W/cm·K	3.8	0.05	0.01	0.05	2.0	1
σ	S/cm	6.0×10^5	1.0	0	0.038	3.8×10^5	1, 3
ε_e			0.357	0.724	0.444		3
ε_p			0.146	0.276	0.186		3
ε_f			0.026	0	0.073		3
r_s	μm		12.5		8.5		3
$c_{s,max}$	mol/cm^3		0.02639		0.02286		3
θ^o			0.53		0.17		3
D_s	cm^2/s		3.9×10^{-10}		1.0×10^{-9}		3
i_o	A/cm^2		0.11×10^{-3}		0.08×10^{-3}		3
$\alpha_a,\ \alpha_c$			0.5, 0.5		0.5, 0.5		3
U	V		Eq. 7		Eq. 8		3
$\dfrac{\partial U}{\partial T}$	mV/K		0		0		
E_{act,i_o}	kJ/mol		30		30		
E_{act,D_s}	kJ/mol		4		20		
$E_{act,\sigma}$	kJ/mol		0		0		
c_e^o	mol/cm^3		2×10^{-3}				3
D_e	cm^2/s		7.5×10^{-7}				3
t_+^o			0.363				3
κ	S/cm		Eq. 19				3
E_{act,D_e}	kJ/mol		10				
$E_{act,\kappa}$	kJ/mol		20				

[*] Values without a reference are estimated values.

At y = H,

$$-\sigma^{eff}\frac{\partial\phi_s}{\partial y} = I$$

$$\qquad\qquad\qquad\qquad\text{if } x < L_{ca} \text{ or } x > L_{cc} \qquad\qquad [29]$$

$$-\lambda\frac{\partial T}{\partial y} = h(T - T_a)$$

At all other boundaries,

$$\frac{\partial \phi_s}{\partial n} = 0$$

$$-\lambda \frac{\partial T}{\partial \mathbf{n}} = h(T - T_a)$$

[30]

where I is the applied current density, h the convective heat transfer coefficient, and T_a the absolute temperature of surroundings. In Eq. 30, h is equal to zero when heat is dissipated only through the tabs.

Numerical Procedures

The model equations summarized in Table I along with the initial and boundary conditions given by Eqs. 27 through 30 are numerically solved following the procedures detailed in Ref. 7.

RESULTS AND DISCUSSION

Numerical simulations are performed on a large-size lithium-ion cell designed for EV and HEV applications. The cell height is 50 cm, a value similar to that used by Baker and Verbrugge.[1] Other cell geometric data are the same as those given by Doyle et al.[3] The relevant material properties and electrode kinetics data are taken from their work and listed in Table II. The activation energies used in the present simulations are estimated from the data used by Botte et al.[4]
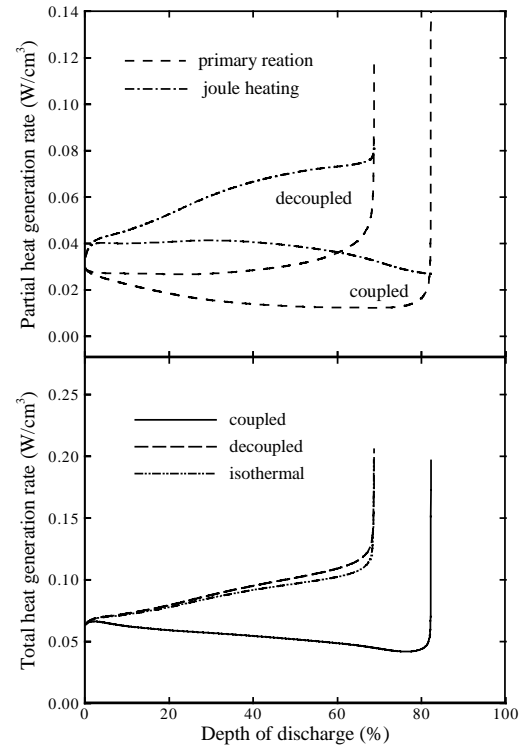
Coupled *vs*. decoupled models

To demonstrate the need for a thermal and electrochemical coupled model in order to accurately predict the electrical and thermal behaviors of Li-ion batteries, Figure 2 compares cell potential and temperature predicted by the coupled and decoupled models, respectively. The decoupled model assumes that all physicochemical properties are temperature-independent so that the electrochemical submodel depends upon temperature only through the Bulter-Volmer equation, Eq. 3. The cell is adiabatically discharged at a constant rate of 3C. A lumped thermal model is used for these simulations in view of the fact that Biot number is equal to zero under the adiabatic condition, thereby justifying that the lumped-parameter approach is applicable. The cell potential and temperature predicted under an isothermal condition are also plotted in the figure for comparison. The decoupled model results are significantly different from the coupled ones, clearly indicating the need to account for thermal-electrochemical coupling in a battery model. Specifically, the decoupled model underpredicts the cell potential and overpredicts the cell temperature. The depth of discharge (DOD) at the end of discharge predicted by the decoupled model is the same as that in the isothermal case, while the coupled model predicts an improved cell capacity, i.e. higher cell potential and greater final DOD, due to improved electrode processes at elevated temperatures.

Figure 3 displays the partial and total heat generation rates during 3C discharge. The total heat generation rate results from the electrode reaction and joule heating. Figure 3 shows that the decoupled model predicts a continually increased total heat generation rate, while the coupled model forecasts a gradually decreased total heat generation rate until the final abrupt rise due to the sharp increase of surface overpotential for the

electrode reaction at the end of discharge. Electrode reactions are greatly facilitated by the increasing cell temperature. Species transport is also enhanced at elevated temperatures. As a result, the cell internal resistance decreases with DOD and hence the heat generation rate decreases.
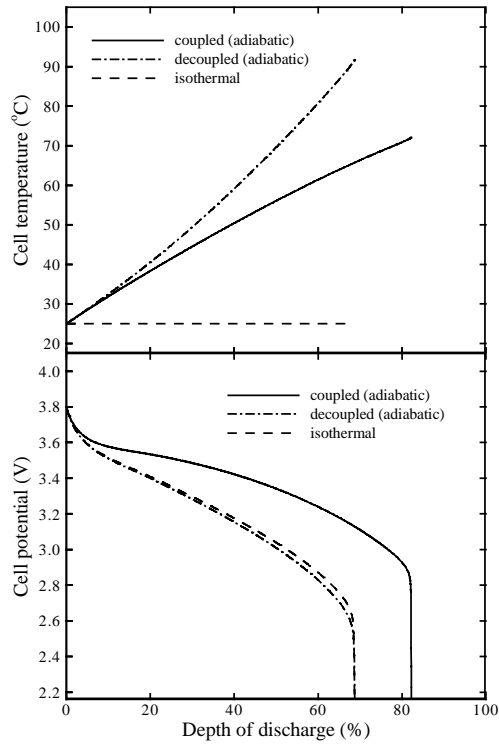

Fig. 2. Cell potential and temperature evolutions during 3C discharge. Comparisons between the coupled and decoupled models

Fig. 3. Partial and total heat generation rates during 3C discharge. Comparisons between the coupled and decoupled models.
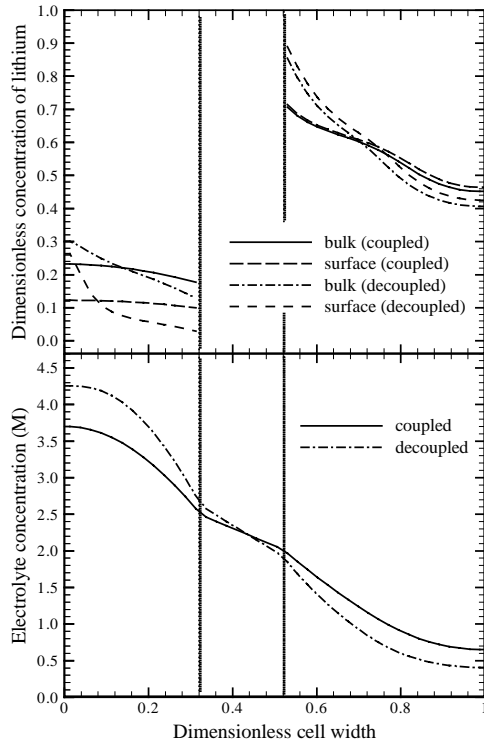
Fig. 4. Concentration profiles of the electrolyte and solid-state lithium at 60% DOD during 3C discharge. Comparisons between the coupled and decoupled models.
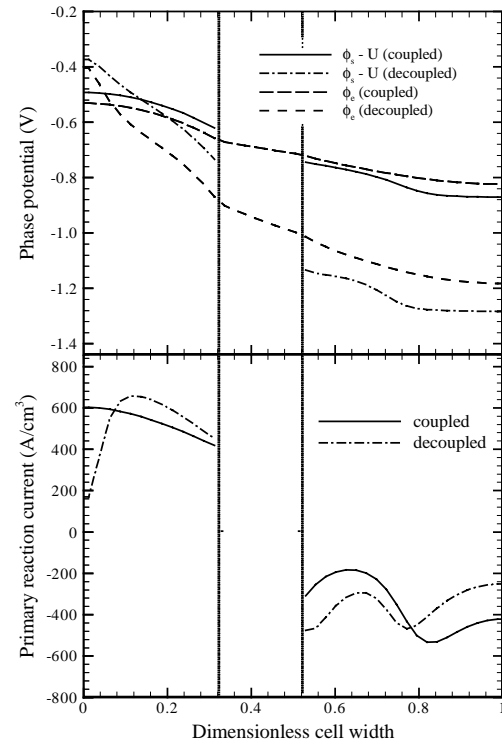
Fig. 5. Distributions of the phase potentials and primary current at 60% DOD during 3C discharge. Comparisons between the coupled and decoupled models.

The decrease in the joule heating with the DOD can be explained by the enhancement in species transport due to increasing temperature, as shown in Fig. 4. The species concentration profile is more uniform in the coupled model than in the decoupled model. This is because the species mass diffusivity increases with temperature in the former case, facilitating species transport. The performance of a Li-ion battery can be limited by lithium diffusion either in the electrolyte or in solid active materials, whichever comes first. It is due to faster species transport at elevated temperatures that the coupled model yields the superior performance mentioned earlier. The ionic conductivity of the electrolyte is also a strong function of temperature. It increases with temperature, causing a reduction in joule heating. Figure 5 shows that the decrease in the surface overpotential contributes to the reduced heat generation rate due to electrode reactions. It also indicates that the phase potentials are greatly flattened because of higher ionic conductivity. As a result, the electrode reaction rate becomes more uniform.

It can be concluded that the decoupled model yields significant errors in the prediction of not only cell electrical and thermal performance but also the internal concentration and electrode utilization. In what follows, the coupled model is used to explore the two-dimensional behaviors of the Li-ion cell.

Two-Dimensional Behaviors

Figure 6 exhibits the cell potential and average temperature evolutions during 3C discharge under various thermal conditions. The cell performance is bounded by two limiting cases: isothermal and adiabatic conditions. The difference in the end DOD is about 14% between the two. Compared to the isothermal case, the cell potential is higher and the final DOD is increased by more than 10% when the generated heat is dissipated

only through the tabs on the top, accompanying by about 40°C increase in the average cell temperature. When the temperature of surroundings is high, the heat effect of side reactions ignored in the present work may become significant.[3] As a result, the cell temperature will further increase and eventually cause thermal runaway. Active thermal management must be carefully considered in order for the large-size Li-ion battery to operate safely. When heat can be dissipated through the sides of cell in addition to the tabs, the cell temperature rise can be reduced within 15°C, with an equivalent convective
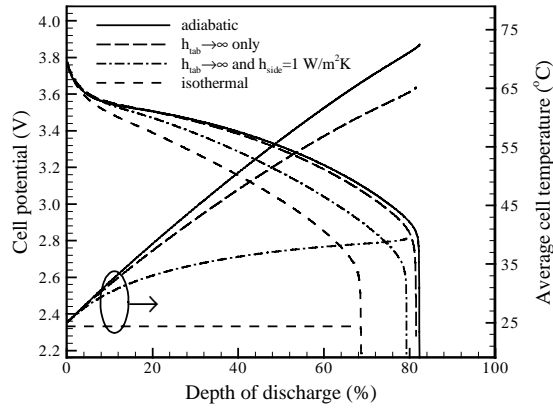
Fig. 6. Cell potential and average temperature evolutions during 3C discharge predicted by the 2D thermal-electrochemical coupled model. Cell width = 0.042 cm and height/width = 1190.
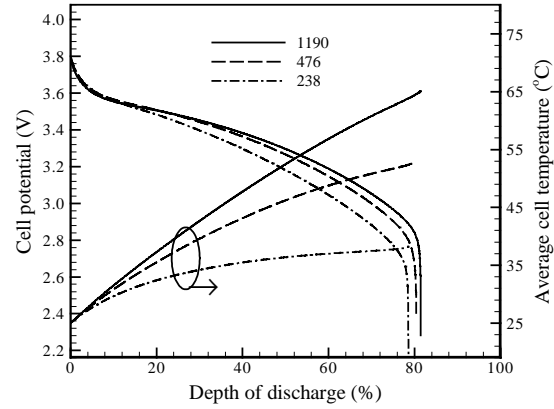
Fig. 7. Effect of the aspect ratio (height/width) on the cell potential and average temperature evolutions during 3C discharge. Cell width = 0.042 cm and heat is dissipated only through tabs ($h_{tab} \rightarrow \infty$).
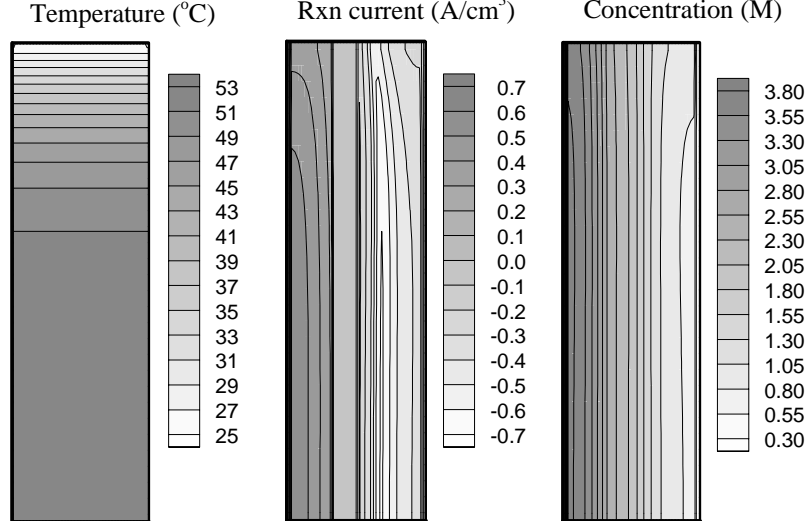
Fig. 8. Contours of the temperature, reaction current, and electrolyte concentration at 45% DODduring 3C discharge. Cell width = 0.042 cm and height/width = 1190. Heat is dissipated only through the tabs ($h_{tab} \rightarrow \infty$).

heat transfer coefficient of 1 W/m²·K for the side cooling. Heat dissipation via the sides of cell becomes difficult in the case of a number of cells stacking together to meet the specific requirements for EV and HEV applications. Nevertheless, it is much more efficient because of the large cooling surface area available at the sides.

Figure 7 shows the effect of cell aspect ratio (i.e. height/width) on the cell potential and temperature evolutions during 3C discharge. Smaller aspect ratio yields a smaller temperature rise. For a fixed cell capacity, a reduction in the cell aspect ratio means a relatively large cooling surface area available through the tabs on the top.

Temperature gradients develop along the cell height during discharge. The maximum spatial temperature variation within the cell is as high as 40°C at the 75% DOD, while it is only 10°C at 15% DOD. Such a large temperature gradient results in severe non-uniformity in the electrode reaction rate along the cell height. The concentration of electrolyte is no longer uniformly distributed along the cell height. Figure 8 displays the contours of cell temperature, electrode reaction rate, and electrolyte concentration at 45% DOD. Apparently, it is inappropriate to assume that the thermal and electrochemical behaviors of a large-size cell are one-dimensional in this situation.

CONCLUSIONS

A multi-dimensional thermal and electrochemical coupled model has been applied to study the discharge of Li-ion batteries. The solid-state lithium diffusion was considered. Local heat generation rate in the cell contributes to the electrode reaction and joule heating in both solid and electrolyte phases. Numerical simulations were performed on a large-size Li-Ion cell for EV and HEV applications. Comparisons between the coupled and decoupled model predictions indicated that a thermal and electrochemical fully coupled model is necessary for accurate prediction of the thermal and electrical behaviors of the Li-Ion cell. Numerical results showed that large temperature gradients develop within the cell along its height, causing severe non-uniformity in both electrode reaction rate and electrolyte concentration. Two-dimensional effects may not be ignored in large-size batteries. In addition, evolutions of cell potential and temperature are greatly affected by the thermal environment and the cell aspect ratio.

ACKNOWLEDGEMENTS

LIST OF SYMBOLS

a_s	specific surface area active for an electrode, cm^2/cm^3
c	volume-averaged concentration of lithium in a phase, mol/cm^3
$\bar{c}_{se}$	area-averaged concentration of solid-state lithium over s-e interface, mol/cm^3
c_p	specific heat, J/kg·K
D	diffusion coefficient of lithium species, cm^2/s
E_{act}	activation energy, J/mol
F	Faraday's constant, 96,487 C/mol
$f_\pm$	mean molar activity coefficient of the electrolyte
h	equivalent convective heat transfer coefficient, $W/cm^2 \cdot K$
I	applied current density, A/cm^2

i	current density vector in a phase, A/cm^2
$\bar{i}_n$	transfer current density of an electrode reaction, A/cm^2
i_o	exchange current density of an electrode reaction, A/ cm^2
j	reaction current resulting in production or consumption of a species, A/ cm^3
L	cell width, cm
L_i	thickness of cell component, μm
l_{se}	diffusion length of lithium from s-e interface into solid phase, cm
q	volumetric heat generation rate, J/cm^3·s
R	universal gas constant, 8.3143 J/mol·K
R_f	film resistance on an electrode surface, Ω·cm^2
r	radial coordinate, cm
r_s	radius of solid active material particles, cm
T	absolute temperature, K
t	time, s
t_+^o	transference number of lithium ion with respect to the velocity of solvent
U	open-circuit potential of an electrode reaction, V
x	coordinate along the cell width, cm
y	coordinate along the cell height, cm

Greek symbol

α_a, α_c	anodic and cathodic transfer coefficients for an electrode reaction
ε	volume fraction of a phase in the REV
η	surface overpotential of an electrode reaction, V
θ	local state of charge evaluated using surface concentration of lithium
κ	conductivity of an electrolyte, S/cm
κ_D	diffusional conductivity of a species, A/cm
λ	thermal conductivity, W/cm·K
ρ	density, g/cm^3
σ	conductivity of solid active materials in an electrode, S/cm
ϕ	volume-averaged electrical potential in a phase, V
Φ	general variable representing a physico-chemical property

Subscript

a	surroundings
as	anode/separator interface
ca	current collector/anode interface
cc	current collector/cathode interface
e	phase of electrolyte
max	maximum value
ref	with respect to a reference state
s	solid phase
se	solid/electrolyte interface
sc	separator/cathode interface

Superscript

eff	effective
Li	lithium species
o	initial value

REFERENCES

1. D.R. Baker and M.W. Verbrugge, *J. Electrochem. Soc.,* **146**, 2413 (1999).
2. T.F. Fuller, M. Doyle, and J. Newman, *J. Electrochem. Soc.,* **141**, 1 (1994).
3. M. Doyle and J. Newman, A.S. Gozdz, C.N. Schmutz, and J.-M. Tarascon, *J. Electrochem. Soc.*, 143, 1890 (1996).
4. G.G. Botte, B.A. Johnson, and R.E. White, *J. Electrochem. Soc.*, **146**, 914 (1999).
5. W.B. Gu and C.Y. Wang, "Thermal-electrochemical modeling of battery systems," *J. Electrochem. Soc.*, submitted for publication (1999).
6. C.Y. Wang, W.B. Gu, and B.Y. Liaw, *J. Electrochem. Soc.*, **145**, 3407 (1998).
7. W.B. Gu, C.Y. Wang, and B.Y. Liaw, *J. Electrochem. Soc.*, **145**, 3418 (1998).